Chemical Engineering Science 112 (2014) 15–24

Contents lists available at ScienceDirect

Chemical Engineering Science

journal homepage: www.elsevier.com/locate/ces

An online method to measure mass transfer of slug flow in a microchannel

Chaoqun Yao [a,b], Zhengya Dong [a,b], Yuchao Zhao [a], Guangwen Chen [a,]*

[a] *Dalian National Laboratory for Clean Energy, Dalian Institute of Chemical Physics, Chinese Academy of Sciences, Dalian 116023, China*
[b] *University of Chinese Academy of Sciences, Beijing 100049, China*

HIGHLIGHTS

- Bubble length increase is compared with the two-phase pressure drop.
- A unit cell model is proposed to study the absorption of CO_2 bubbles.
- Bubble size reduction is used to determine the mass transfer coefficient.
- Mass transfer during bubble formation process is measured.
- The effect of fluid properties on the mass transfer is studied.

ARTICLE INFO

Article history:
Received 11 January 2014
Received in revised form
26 February 2014
Accepted 15 March 2014
Available online 21 March 2014

Keywords:
Taylor flow
Gas–liquid
Carbon dioxide
Microreactor

ABSTRACT

Physical absorption of CO_2 bubbles under slug flow has been studied in a T-junction microchannel. Based on the absorption rate of gas bubbles, an online photographic method is proposed to determine the mass transfer coefficients. Validity of this method is verified by evaluating bubble expansion due to pressure drop and by comparing the results with literature. The effect of fluid properties on the mass transfer has also been studied with ethanol solutions, which shows that mass transfer coefficient increases with the increase of ethanol concentration. The amount of gas absorbed during the bubble formation process has been measured to be about 2–10% of the inlet gas phase, and is found to linearly scale with the maximum mass transfer rate. For each fluid system, the initial dissolution rates of bubbles differ very little for short contact distance, whereas, the final amount of dissolution only depends on the residence time.

1. Introduction

Microreaction technology has gained increasing attention on the improvement of multiphase processes over the recent years. High mass and heat transfer rate are obtained in microreactors due to large and controllable surface area to volume ratio (Yue et al., 2007; Cao et al., 2010), which is pretty important for multiphase processes. Key features of these novel reactors include miniaturization and numbering up mode, leading to a great reduction in investment of both expenses and time from lab research to industrial application. Additional benefits include better process safety via excellent thermal management (Cao et al., 2010), low material hold-up, sharp residence time distribution (Günther et al., 2004) and high volumetric productivity.

When gas and liquid flow through microchannels, a stable slug flow or Taylor flow (Triplett et al., 1999; Zhao et al., 2013) is obtained within a large range of operating conditions. The slug flow is characterized by sequences of an elongated gas bubble and a liquid slug. If the channel wall is wetted by the liquid phase, the gas bubbles are separated from the wall by a thin liquid layer (Fries et al., 2008b; Thulasidas et al., 1995). Slug flow is considered as a promising flow pattern to improve reaction performance for many reasons: uniformly dispersed gas bubbles, fixed gas–liquid interface, narrow residence time distribution, enhanced mass or heat transfer due to inner recirculation of liquid slugs and flexible operating conditions. Up to now, wide attention has been paid to slug flow on various aspects such as bubble formation process and bubble length (Dang et al., 2013; Garstecki et al., 2006; van Steijn et al., 2007), bubble shape and liquid film distribution in the cross section (Fries et al., 2008b; Han and Shikazono, 2009; Kreutzer et al., 2005a; Thulasidas et al., 1995), gas hold-up or void fraction (Kawahara et al., 2005; Xiong and Chung, 2007), pressure drop (Kreutzer et al., 2005a,b; Yue et al., 2009) and so on. Even for some major drawbacks that hinder the

---

* Corresponding author. Tel.: +86 411 8437 9031; fax: +86 411 8469 1570.
E-mail address: gwchen@dicp.ac.cn (G. Chen).

http://dx.doi.org/10.1016/j.ces.2014.03.016
0009-2509/

large scale application of microreactors such as distribution of multichannels (Al-Rawashdeh et al., 2012, 2013) and short residence time/reaction time (Hessel et al., 2013), significant progress has been made.

Mass transfer characteristics of gas–liquid slug flow in microchannels have also been a hot subject in literature (Berčič and Pintar, 1997; Ganapathy et al., 2013; van Baten and Krishna, 2004;Vandu et al., 2005; Yue et al., 2007). Earlier work was carried out experimentally in capillaries with different diameters by Berčič and Pintar (1997), who found that the overall liquid side volumetric mass transfer coefficient is related to flow details such as bubble velocity and bubble length. Sobieszuk et al. (2011) used the Danckwerts Plot to simultaneously measure the interfacial area and liquid side mass transfer coefficient, which showed dependency on contact time. As recently reviewed by Sobieszuk et al. (2012), most of the works deal with quantification of mass transfer and building empirical correlations for predicting them while less attention has been paid on the effect of fluid properties on mass transfer characteristics. Fluid properties such as viscosity and surface tension have a large effect on the hydrodynamics, they are due to the effect of mass transfer, too. Therefore, research on influences of fluid properties on mass transfer characteristics is of great importance. The practical meaning is also obvious as fluid properties vary largely in practical gas–liquid processes. However, classic methods, which usually consist of measuring the gas and/or liquid composition, are rather time-consuming since flow rates in single microchannel usually range from a few μL/min to several mL/min. Also, these conventional methods still face other problems including saturation problems (Pohorecki, 2007) and serious end effects (Sobieszuk et al., 2011; Yue et al., 2007), which originate from large contribution of the inlet, outlet and gas–liquid separation sections. Online methods serve as good solutions (Dietrich et al., 2013; Tan et al., 2012b) to avoid these problems. Tan et al. (2012b) developed an online method to determine the mass transfer by measuring the change of CO_2 bubble volume under absorption of NaOH solutions. Recently, Dietrich et al. (2013) developed a new colorimetric technique to measure the concentration distribution in the liquid slugs. Through this way, not only overall mass transfer is calculated, but also spatial information is obtained to visualize the locations where the mass transfer from gas bubbles happens. However, the above methods are only suitable for specific fluid systems with chemical reaction and the chemical enhancement factor is not separated. Therefore, developing novel online method that can directly measure the mass transfer coefficients is of great importance.

In this work, an online method based on the physical dissolution rate of bubbles is proposed to measure the mass transfer of slug flow in a rectangular microchannel. In the first part, the principle of the method is illustrated and verified by comparing the mass transfer coefficients with literature. Then pure CO_2 is used to analyze absorption process with different liquid absorbents in the microchannel. Information about mass transfer coefficients, bubble and slug length, absorption during bubble formation process, dissolution rate will be presented and discussed.

2. Experimental section

Gas–liquid slug flow was generated in a rectangular cross-section microchannel with a crossing T-junction. The main channel has a meandering form with right angled bends as shown in Fig. 1. All the channels have the same width of 600 μm and depth of 300 μm. The entire length of the main channel is about 150 mm. The channels were fabricated on a polymethyl methacrylate substrate (PMMA, A grade, 92% of light transmittance, ShenZhen HuiLi Acrylic Products Co., Ltd.) using micromachining technology (FANUC KPC-30a) in our CNC Machining Center. The reactor was sealed by screws.

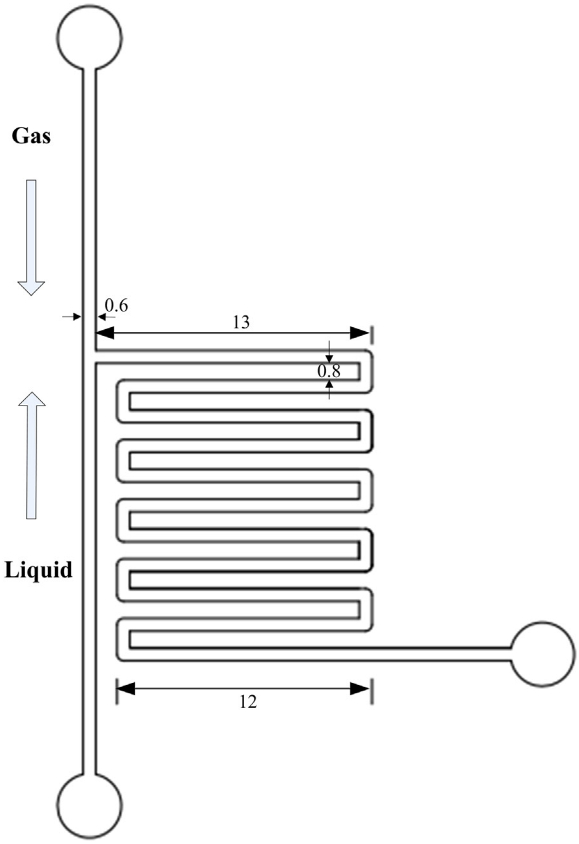

Fig. 1. Schematic diagram of the gas–liquid microchannel contactor.

Gas flow was provided via a pressure regulator and controlled by a mass flow controller (D07-19B, Beijing Sevenstar Electronics Co., Ltd., China) with an accuracy of 0.5% full scale. Liquid flow was pumped by a high precision digital piston pump (Series II, Chrom. Tech. Inc.). The actual flow rate under each run was determined by a weighing method. In order to eliminate the pulsation of the liquid flow rate, a buffer tank was introduced before the microreactor inlet. After flowing through the microchannel contactor, gas and liquid were separated in a gas–liquid separator. The pressure drop between the gas inlet and the outlet was directly recorded by a differential pressure transducer. All experiments were conducted under ambient conditions. Detailed information about the experimental setup is available in our previous work (Yao et al., 2013). The liquid phase used here was water–ethanol mixtures with different content. The fluid properties are displayed in Table 1.

To study the flow and absorption characteristics of slug flow, the flow pattern was recorded by a CMOS high-speed camera system (BASLER A504kc) with a macrolens (Nikon AF Micro-Nikkor 2,8/60 mm). The CMOS camera was placed above the visual window and strong light was provided by a cold light source. In all experiments, the CMOS camera was set to work at a recording rate of 640 frames/s and a resolution of 1280 × 800 pixel^2. The shutter time was set as 80 μs. A moderate amplification of the images was chosen to have one pixel representing about 15 μm. With a Matlab program (Yao et al., 2013), we can obtain flow information such as bubble lengths, bubble velocities, bubble locations and so on. Under each operating condition, a sequence of at least 200 images was analyzed and the data were averaged to obtain the final value. The relative standard deviation (RSD) of the bubble and slug length did not exceed 5%. In our work, the picturing zone can only cover the first 8 channels with a length of about 100 mm. So the flow pattern in the last channel length (4–11 channels,

Table 1
Fluid properties of ethanol–water solutions, diffusion coefficients and solubility of CO_2 in corresponding liquids at 22 °C.

	Ethanol content (wt%)						
	0	10	30	50	70	90	100
ρ (kg m^{-3})	998	982	954	912	868	818	791
μ (mPa s)	1.003	1.375	2.480	2.971	2.572	1.745	1.189
σ (mN m^{-1})	72.75	48.14	33.53	28.51	25.48	23.23	22.31
D (10^{-9} m^2 s^{-1})	1.954	1.616	1.368	1.619	2.356	3.527	4.397
C^* (mol/L)	0.03349	0.03239	0.02989	0.03781	0.06277	0.08111	0.1248

Note: density, viscosity and surface tension data are from Khattab et al. (2012); diffusion data are from Simons and Ponter (1975); solubility data are from Dalmolin et al. (2006).

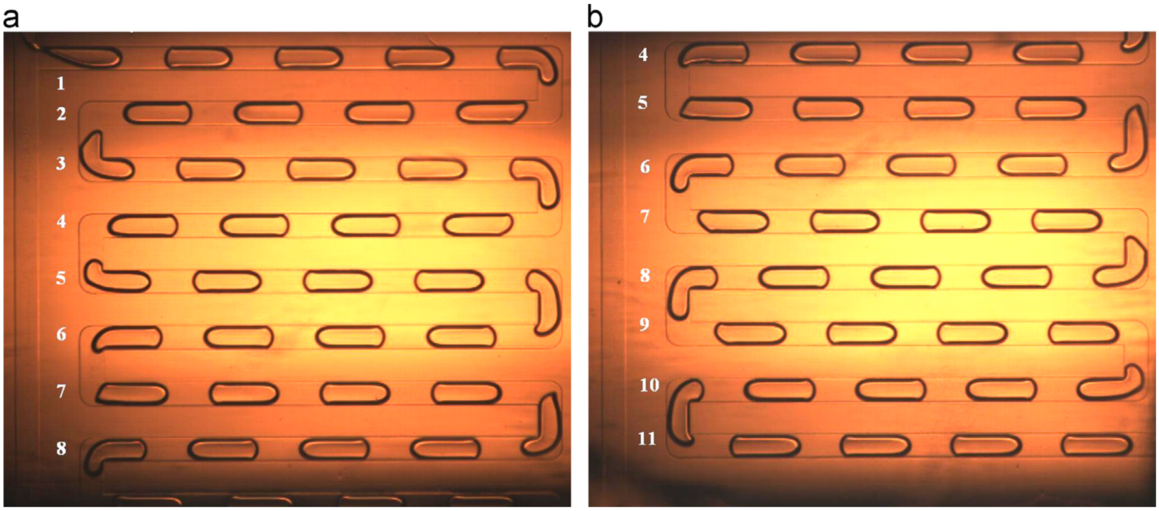

Fig. 2. Typical slug flow pattern of N_2-H_2O, Q_G=2.0 mL/min, Q_L=1.5 mL/min (a) image captured for 1–8 channels (b) image captured for 4–11 channels.

50–150 mm) was captured by moving the reactor for a second picturing. As the system is very stable, the consistency of the flow pattern between the two picturings is good. It is further guaranteed by the short time interval, which was less than 30 s. A typical set of captured images is shown in Fig. 2. As can be seen, the flow patterns in the middle of the reactor (4–8 channels, 50–100 mm) for the two picturings are almost the same.

3. Online method for determination of mass transfer coefficient under physical absorption

3.1. Pressure drop analysis

In this work, the mass transfer coefficient was determined by an online method, which is based on the bubble size reduction along the channel lengthwise direction. Before application of this method, the bubble expansion effect due to pressure drop has to be evaluated and minimized. It is also very important for other applications, such as determination of solubility (Abolhasani et al., 2012) and reaction kinetics (Li et al., 2012), because the net reduction of the bubble size is needed. Here, a comparison between increase in the length of gas bubbles and pressure drop is presented in Fig. 3 for pure gas–liquid slug flow without absorption. The initial gas bubble length L_{B1} was determined as the lengths of the bubbles right after the acquisition of their regular shape. As can be seen, the decrease in the pressure leads to a larger bubble length, yet, with limited effect. According to the ideal gas law, the y-axis value $\Delta L_B/L_{B1}$ should be equal to the x-axis value $\Delta P/P_a$ if the pressure drop in a single bubble is the same as the total pressure drop of the gas–liquid two phase flow. However, most of the data in Fig. 3 lie below the quarter line (y=0.5x), indicating that the pressure drop in a single gas bubble is much smaller than the total pressure drop over the microchannel reactor. This also means that the pressure inside a gas bubble is always much larger than that in the liquid phase near the bubble cap due to the Laplace pressure, which is verified by many numerical research studies (Abadie et al., 2012; Kreutzer et al., 2005b). It is clear that even though the total pressure in the present reactor is larger than that in straight channels, the bubble expansion may still be very small. As a result, it is reasonable to neglect the bubble expansion, provided the total pressure drop is small enough.

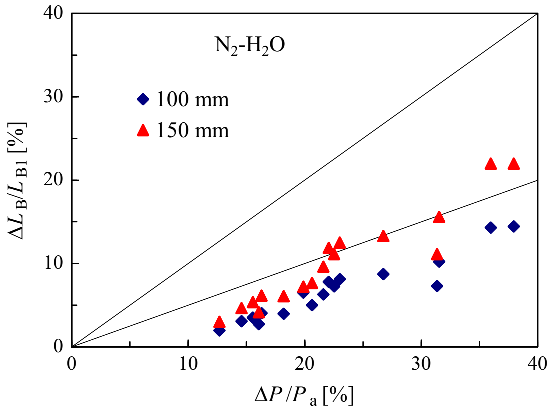

Fig. 3. The increase in bubble length at locations of 100 mm and 150 mm downstream the T-junction versus the total pressure drop over the reactor. The fluids are N_2 and H_2O.

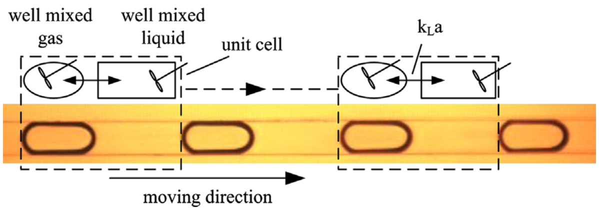

Fig. 4. Schematic representation of the unit cell model for determining k_La values.

3.2. Unit cell model

In order to determine the liquid side mass transfer coefficient, a unit cell model was proposed here similar to the model of Vandu et al. (2005), as shown in Fig. 4. The model is based on the following assumptions:

- In each unit cell, gas and liquid phases are both well mixed, respectively.
- Mass transfer from gas to liquid phase only happens in a single unit cell.
- No mixing happens between different unit cells.

Then the mass transfer of gas bubbles can be correlated with bubble shrinkage rate by the Lagrange method. Mass balance of gas phase in a single unit cell can be obtained as

$$\frac{dV_B}{dt}=\frac{dV_B}{dx}U_B=-k_La(C^*-C)V_L\frac{RT}{P} \tag{1}$$

where V_L and V_B denote the volume of liquid and gas bubble in a single unit cell. As indicated by Berčič and Pintar (1997) and Yue et al. (2007), mass transfer coefficient is calculated based on the following equation:

$$k_La=\frac{j_L}{x}\ln\left(\frac{C^*-C^0}{C^*-C}\right) \tag{2}$$

Then the concentration of solutes in the liquid phase in a microchannel is calculated as

$$C^*-C=(C^*-C_0)e^{-x/j_L\ k_La} \tag{3}$$

where C_0 is the liquid concentration at x_0 and equals 0 if x_0 is at the T-junction where gas and liquid starts to contact. During slug flow, bubble shape in the cross section does not change at all, so the bubble volume can be treated to linearly scale with its length and $dV_B/dx=A_BdL_B/dx$. This assumption is well satisfied when the bubble length is very large but would induce larger error when bubble length is close to the channel width. So the experimental data for analysis were carefully chosen to avoid/reduce the error as much as possible. With the bubble velocity replaced by the logarithm average bubble velocity, Eq. (1) can be solved with Eq. (3) and gives

$$L_B=L_{B0}+\frac{C^*-C_0}{U_BA_B}V_L\frac{RT}{P}j_L(e^{-x/j_L\ k_La}-1) \tag{4}$$

This equation indicates that the relationship between bubble length and their location follows an exponential type:

$$L_B=m_1+m_2e^{-m_3x} \tag{5}$$

The physical meaning of m_1 is the final bubble length when the liquid phase is saturated and the meaning of m_1+m_2 is the initial bubble length generated. By fitting the bubble length at different locations, the liquid side volumetric mass transfer coefficient k_La can be determined. An advantage of this method is that there is no need to exclude or approximate the end effects resulted from gas absorption during the formation process and the outlet section (Sobieszuk et al., 2011; Yue et al., 2007), which is important in determining mass transfer coefficient in microchannels. The absorption of CO_2 into water is used as the working fluid to test the validity of this online method. Only conditions with pressure drop less than 16 kPa ($\Delta P/Pa < 16\%$) were chosen for analysis to ensure the bubble expansion effect ($\Delta L_B/L_{B1} < 3.5\%$) can be neglected. Fig. 5 shows an exemplary fitting of the model. An excellent fitting performance can be observed.

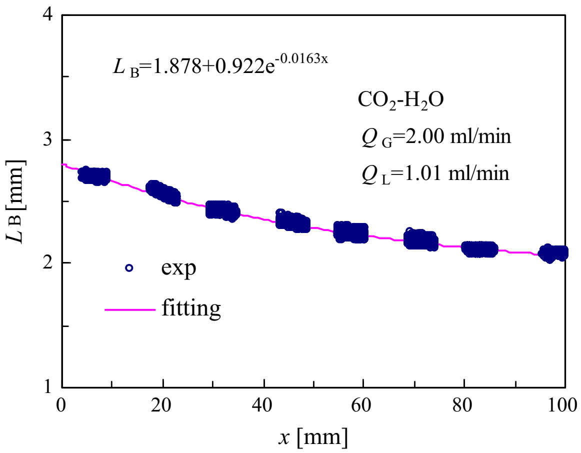

Fig. 5. Exemplary fitting data for physical absorption.

It should be noted that the mass transfer enhancement of the bends (Fries et al., 2008a) is included and k_La here is a mean value over the reactor (actually fitting distance). This is a very important hypothesis in the model because k_La actually decreases along the channel length when the bubble size decreases. The dose of hypothesis impact on k_La, k_L and a depends on the content of bubble shrinkage. For those systems with low gas solubility such as CO_2–water, the effect is small as the bubble reduction is very small, whereas the decrease of k_La is larger with high gas solubility. For the interfacial area, the maximum decrease of a in our experiments does not exceed 33% despite the relatively large bubble shrinkage and most data lie between 5% and 20%. It is reasonable because the total volume of the unit cell decreases largely with the decrease in bubble size at the same time. As to the effect on k_L, it may be larger if only bubble velocity is taken into consideration. However, many other factors can also have large effects on k_L. Longer bubbles generally lead to a smaller k_L, due to low mixing efficiency and liquid film saturation. That is why in several research papers a larger gas flow rate does not lead to a larger k_L (Yue et al., 2007; Dietrich et al., 2013; Tan et al., 2012b). Therefore, the decrease of k_L is also limited. So in general, the hypothesis can be justified to some content and the model is applicable.

3.3. Verification of online method by comparison with literatures

Fig. 6(a) depicts the measured k_La as a function of the gas–liquid flow rate ratio at the inlets. The error bar was based on the calculations of k_La by revising bubble length with the total pressure drop and the ideal gas law, although we have illustrated that the effect of the total pressure drop on the bubble length is much smaller than expected. It can be seen that k_La increases either with increasing gas flow rate or liquid flow rate. The effect of liquid flow rate is more obvious than the effect of gas flow rate, which was also reported by Yue et al. (2007). A comparison of the present results with those obtained with the correlations in the literatures (Berčič and Pintar, 1997; Vandu et al., 2005; Yue et al., 2007, 2009; Kuhn and Jensen, 2012) is shown in Fig. 7. The predictions of Berčič and Pintar (1997) and Vandu et al. (2005) deviate a lot from our results while those of Yue et al. (2007, 2009)

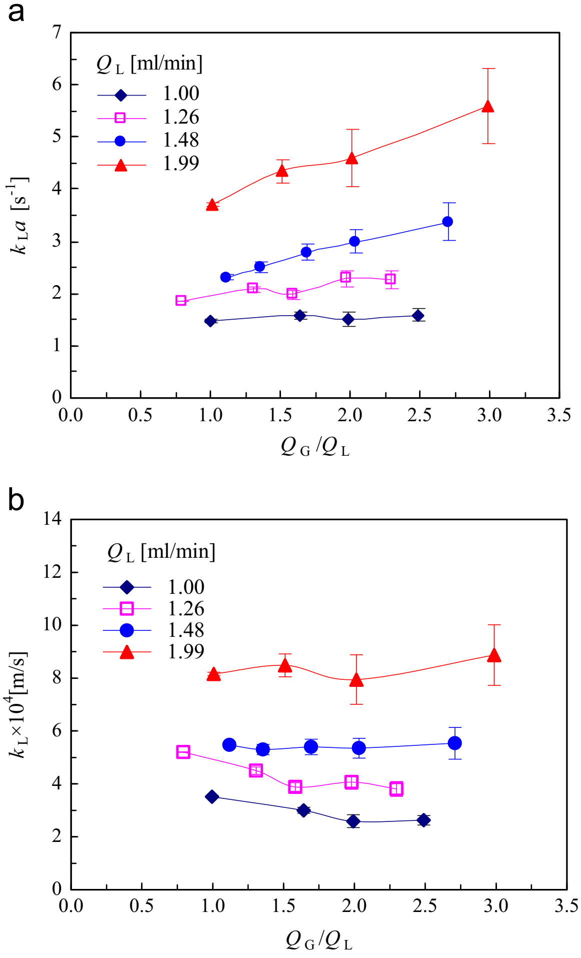

Fig. 6. (a) Volumetric liquid side mass transfer coefficient (b) liquid side mass transfer coefficient versus flow rate ratio for CO_2–H_2O system.

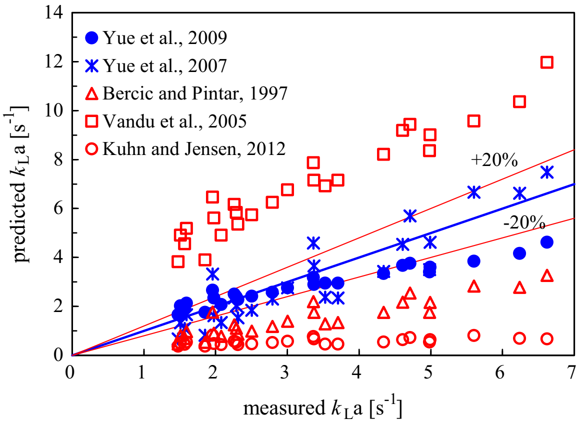

Fig. 7. Comparison of k_La with predictions of correlations in literatures.

are much closer. The present results here are also very close to the results determined with the Danckwerts Plot method in a recent work of Sobieszuk et al. (2011) in which the microchannel size and flow rates were similar to ours. In the more recent work of Kuhn and Jensen (2012), they also used meandering channels of similar channel size, but their correlation far under predicts our results. This is probably due to their very low gas or liquid flow rates compared to our system.

The recorded pictures of slug flow allows determination of the specific surface area (a) for each experimental condition (Sobieszuk et al., 2011) and the calculation method was introduced in detail in our previous work (Yao et al., 2013). Therefore, mass transfer coefficient (k_L) can be evaluated by dividing k_La by a. The results are shown in Fig. 6(b). As can be seen, the values vary from 2×10^{-4} to 9×10^{-4}, which lie in the range of values reported by Yue et al. (2007). It can also be observed that k_L increases with increasing Q_L whereas it slightly decreases with an increase in Q_G when Q_L is small. Similar phenomena were also observed in millimetric capillaries by Dietrich et al. (2013), who determined k_L with concentration distribution in the liquid slugs. According to the penetration theory, k_L is related to the contact time of fluid elements at the gas–liquid interface. So a higher gas flow rate, which leads to a higher inner recirculation of the liquid slugs (Zaloha et al., 2012), should result in a shorter contact time and therefore a larger k_L. Since k_L here is determined based on the widely used unit cell model (Dietrich et al., 2013; Vandu et al., 2005; Yue et al., 2009) in which the liquid is treated as a stirred tank reactor, the decrease in k_L may be explained by mixing efficiency in a single unit cell. As Q_G increases, shorter liquid slug and longer gas bubble are obtained. Then the mixing between liquid in the slug and the liquid film between the gas bubble and channel wall is slowed down, leading to a smaller k_L. By comparison of k_L and k_La with literatures, it can be concluded that the online method is able to measure the mass transfer coefficients under slug flow.

4. Applications, results and discussion

4.1. Mass transfer coefficients under different ethanol solutions

Although plenty of research studies have been dedicated to determine mass transfer coefficients and many correlations have been developed, the knowledge of the effect of fluid properties on mass transfer is lacked, especially the gas solubility. Here, CO_2 absorption with water–ethanol mixture is chosen to improve the understanding because ethanol is cheap and non-toxic and most important of all, the physical or chemical properties of water–ethanol mixture are relatively easy to find out. Fig. 8 shows the comparison of volumetric mass transfer coefficients among different ethanol solutions. It can be seen that larger k_La was obtained with higher concentrations of ethanol. A higher concentration of ethanol would also lead to a larger k_L, as shown in Fig.9. However, the independent effect of fluid properties such as surface tension and viscosity cannot be directly observed from the results here. This is because it is impossible to vary one parameter without changing another. Moreover, changing fluid properties also has a great influence on the flow behavior. Since convective mass transfer and mixing play more important roles than diffusion (Dietrich et al., 2013), the relationship between mass transfer coefficients and ethanol concentration can be explained by the hydrodynamics, which are displayed in Fig. 10. As can be seen, both gas bubbles and liquid slugs are shorter at higher concentrations of ethanol solutions due to their relatively high viscosity and low surface tension, which both lead to a faster generation of gas bubbles (Dang et al., 2013; Qian and Lawal, 2006). The generated gas bubbles also move faster when the ethanol concentration is higher. These characteristics make the results of mass transfer coefficients reasonable since it is well known that shorter gas bubbles and liquid slugs and higher bubble velocity are all beneficial for fast mass transfer rate (Yue et al., 2009; Vandu et al., 2005; Zaloha et al., 2012). Shorter bubbles can avoid saturation of the liquid film between the gas bubbles and the channel wall (Pohorecki, 2007; Yue et al., 2009) and also increase the mixing between the liquid film and the liquid slug. This is in accordance with the results that k_L for ethanol solutions increases with the increase in gas flow rate, which is different from the

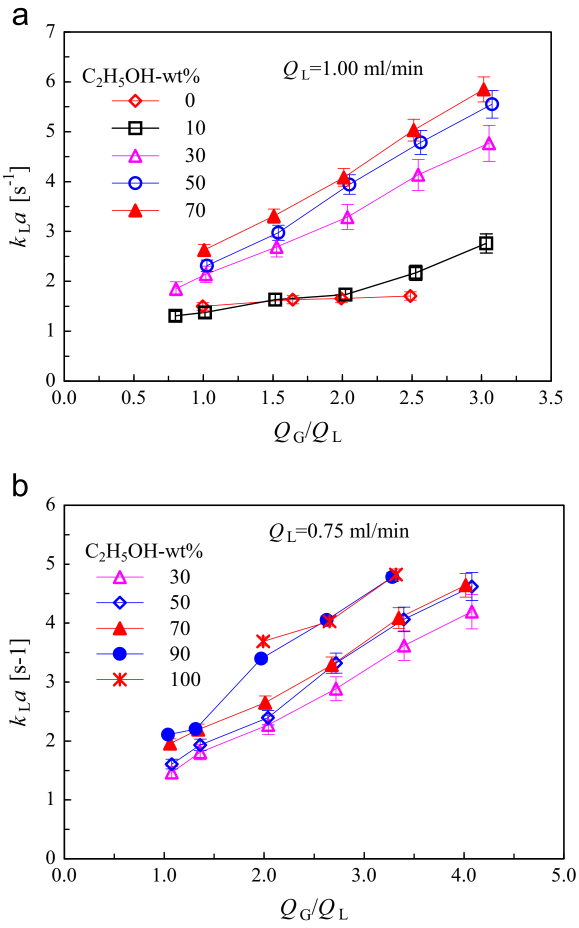

Fig. 8. k_La in aqueous solutions of ethanol.

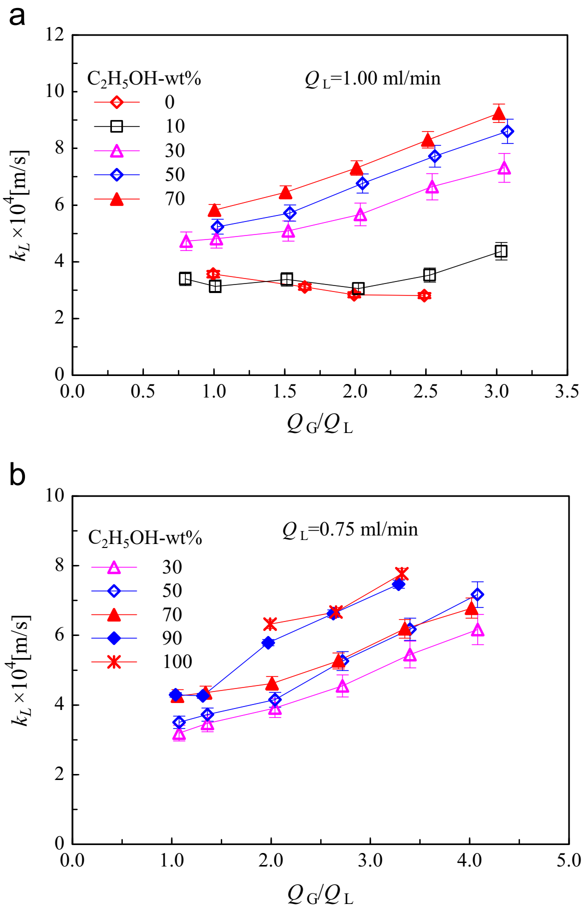

Fig. 9. k_L in aqueous solutions of ethanol.

situation of CO_2–water system. For the shorter liquid slugs, a higher inner recirculation rate can be obtained, which greatly enhances the mass transfer (Zaloha et al., 2012).

A correlation was developed to estimate the liquid side volumetric mass transfer coefficient as following:

$$Sh_L ad_h = 1.367 Re_G^{0.421} Re_L^{0.717} Sc_L^{0.640} Ca_{TP}^{0.5} \tag{6}$$

where all the dimensionless parameters are based on the inlet conditions. A total of 118 sets of the experimental data were correlated using the Levenberg–Marquardt approach in software 1stOpt. Good fitting performance was obtained with the standard deviation being 0.97, which implies an excellent prediction of Eq. (6), as shown in Fig. 11.

4.2. Amount of gas absorption during gas bubble formation process

Unlike the extensive research studies on the gas–liquid slug flow and reactions, very limited studies have been focused on the mass transfer performance during the bubble formation process. However, it is a very important point in many aspects (Abolhasani et al., 2012; Li et al., 2012; Sobieszuk et al., 2011; Tan et al., 2012a; Yue et al., 2007). For example, Li et al. (2012) had to conduct control experiments with non-reactive fluid for the kinetic study of fast gas–liquid reactions. In order to determine the mass transfer coefficient in microchannels, Yue et al. (2007) developed an antitheses method to eliminate the end effects by using two contactors, which have the same inlet and outlet structure, and differ in whether there is a main channel or not. Some other research studies (Abolhasani et al., 2012) just neglected the inlet effect due to no accurate information to be obtained. Recently, Tan et al. (2012a) determined the amount of CO_2 absorbed by NaOH solution during the formation stage to be around 30% of the total CO_2 in the gas phase. They measured the CO_2 fraction in the gas bubbles by comparing the lengths with their final length in the last channels, in which CO_2 is completely exhausted and only N_2 is left. However, this method is not available if pure gas is involved.

The amount of gas absorption during the gas bubble formation process here is estimated by extrapolating the bubble length right at the T-junction L_{B0} with Eq. (5). The extrapolation was verified by comparing them with the bubble length generated with N_2, as shown in Fig. 12. It can be seen that both the bubble length and the product of bubble length and frequency agree pretty well with that for the N_2 system. The mass transfer distance during formation process is defined as the bubble moving distance in a bubble generation period as

$$x_1 = U_{B0}/f \tag{7}$$

where U_{B0} is the initial bubble velocity and f is the bubble formation frequency. And then the fraction of gas absorbed in the total amount of gas phase during the bubble formation process is obtained as

$$\varphi = 1 - L_B(x_1)/L_{B0} \tag{8}$$

The results are plotted versus the bubble formation period as shown in Fig. 13. Under experimental conditions, the fraction φ ranges from 2% to 10%. These values are far smaller than that obtained by Tan et al. (2012a). It is reasonable since the mass transfer time here is only several milliseconds compared to their much longer time of about 0.2–0.4 s. Another reason is that the enhancement factor of chemical reaction largely increases the absorption rate during bubble formation stage. Our results are close to the simulation results of Ganapathy

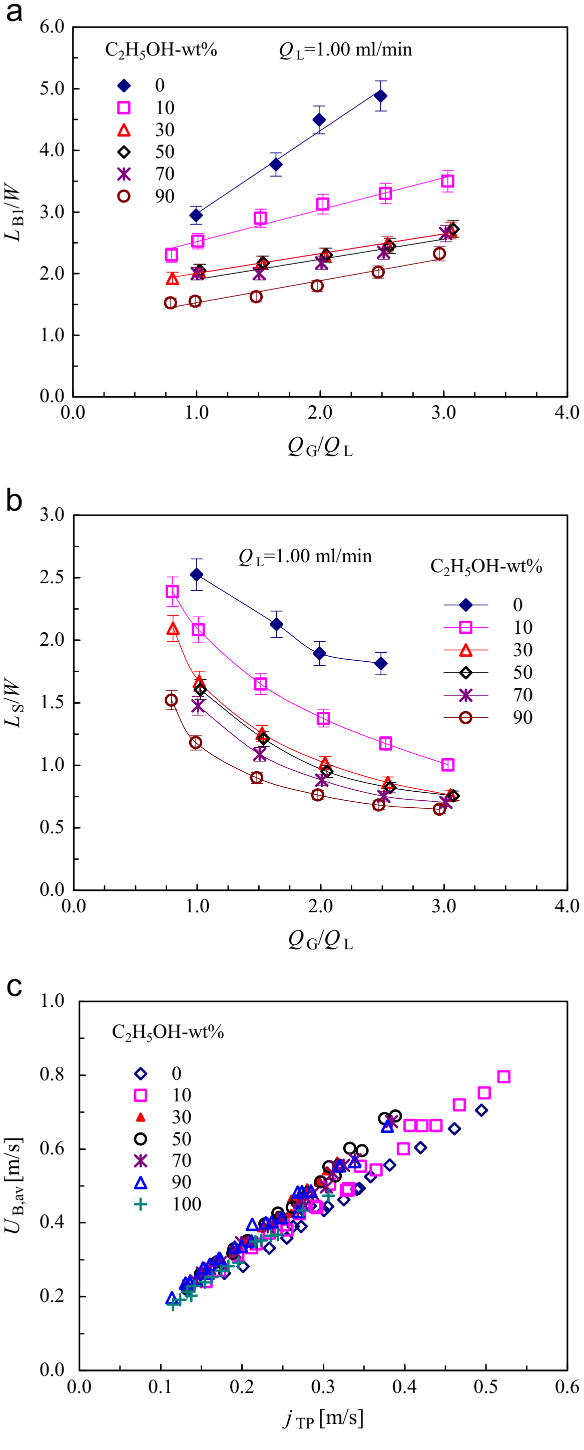

Fig. 10. Flow hydrodynamics of slug flow with different ethanol solutions: (a) the initial bubble length, (b) liquid slug length and (c) average bubble velocities in the first channel.

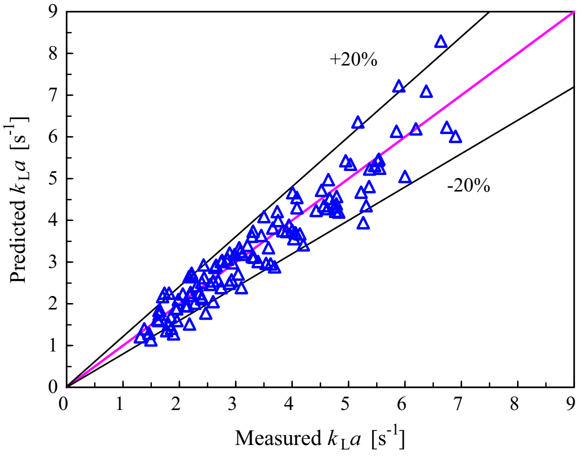

Fig.11. Comparison between the measured liquid side volumetric mass transfer coefficients and the predicted values by Eq.(6).

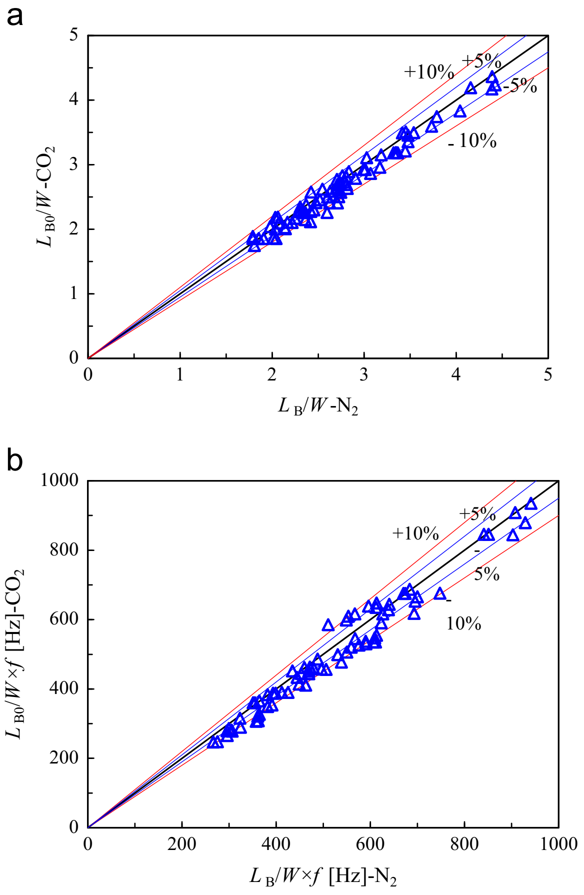

Fig. 12. Comparison of (a) initial bubble length, (b) product of bubble length and frequency between CO_2 and N_2 system for the same gas and liquid flow rates.

et al. (2013), who have shown that the absorption fraction counts about 1.5–3.3% during a formation cycle of about 5–10 ms. The low values here validate the neglect of the inlet effect in the work of Abolhasani et al. (2012). However, for some other applications, this effect may be rather significant (Tan et al., 2012a) and more efforts should be made to investigate the fundamental mechanism in the formation process.

It can also be seen in Fig. 13 that the fraction φ increases with the increase in ethanol concentration. This suggests that the gas solubility plays an important role in gas absorption in the formation stage. When φ is plotted as a function of the maximum mass transferred, $k_L a C^* t$, a linear relationship is observed, as shown in Fig. 14. As the bubble formation time is very small, the concentration of gas solutes is close to zero and therefore the absorption rate can be treated as being constant. This linear relationship can be used to estimate the amount of gas absorbed during the bubble formation process.

4.3. Dissolution rate

A direct observation of gas dissolution is illustrated from the bubble length reduction through the channel as shown in Fig. 15 (a). The data in this figure is obtained from fitting the raw bubble

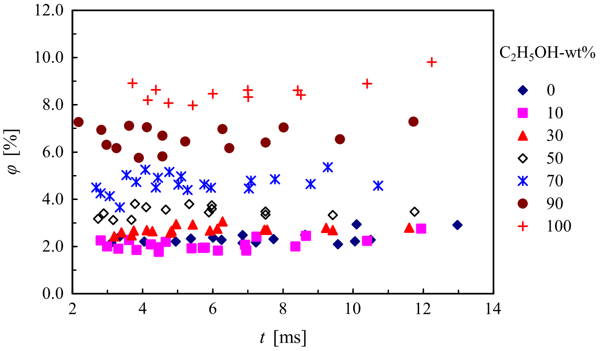

Fig. 13. The fraction of gas absorbed during the bubble formation process versus the formation period.

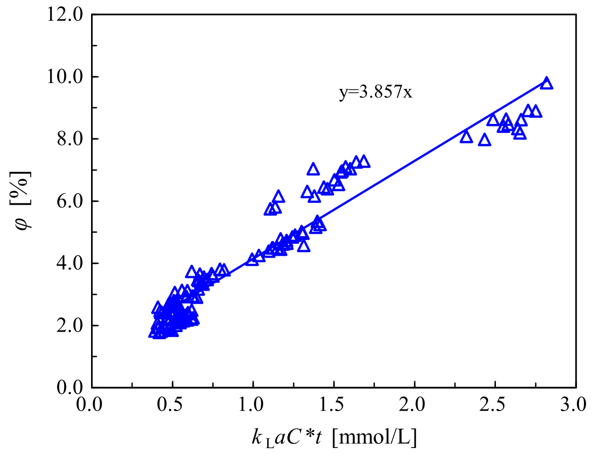

Fig. 14. Evolution of the fraction φ as a function of maximum mass transferred during a bubble formation cycle.

length and the distance using Eq. (5) for esthetics. It can be seen that the bubble length decreases fast firstly and then the rate slows down as the liquid phase is close to saturation and the driving of concentration difference decreases. In contrast to the large decrease in bubble length, the change in liquid slug length at a constant inlet gas flow rate is nearly null (Abolhasani et al., 2012), which means the separation of liquid phase by gas bubbles is still valid. This phenomenon validates the using of the unit cell model (Vandu et al., 2005). Actually, when the segmented slug flow turns into bubbly flow (Cubaud et al., 2012; Yue et al., 2008) due to strong dissolution, the slug length or the spacing between adjacent bubbles only increases a little. In this paper, experimental data were carefully chosen to assure that all the bubble lengths were larger than channel width.

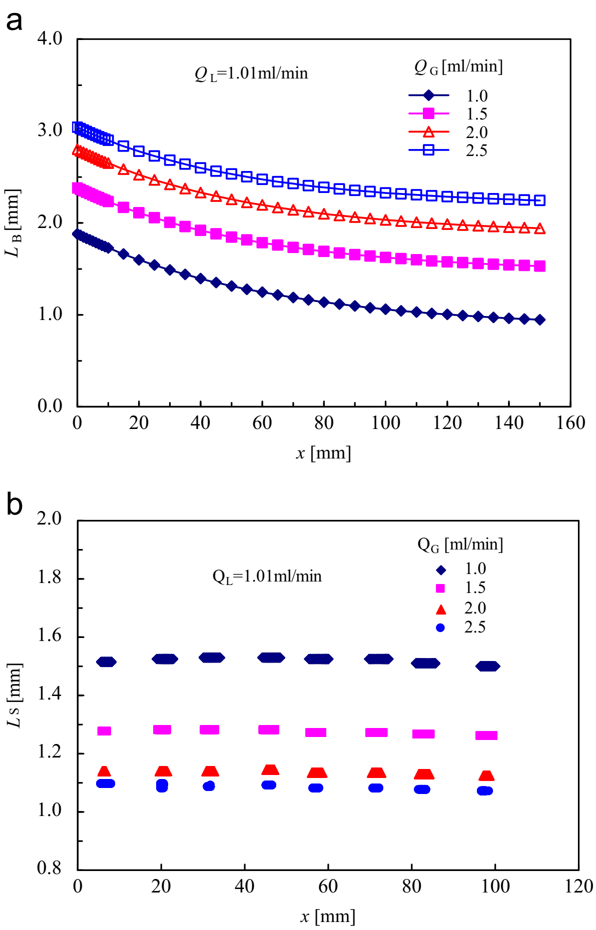

Fig. 15. Evolution of (a) gas bubbles and (b) liquid slugs along microchannel for CO_2–H_2O system.

The dissolution rate does not seem to be significantly influenced by the initial bubble length and the gas flow rates since curves appear parallel. To further investigate the influence of gas and liquid inlet flow rates on the dissolution rate, the bubble size evolution L_{B0}-$L_B(x)$ is plotted in Fig. 16, which shows the absolute amount of CO_2 absorbed in a single unit cell along the channel length. As can be seen, the curves collapse on a single one (Sun and Cubaud, 2011) when the mass transfer distance is less than about 40 mm in the fast mass transfer zone, indicating very little difference in the amount of CO_2 absorption into liquid between different operating conditions. This clearly confirms the findings of Zaloha et al. (2012), namely that the amount of heat or mass transferred between gas and liquid phases in a unit cell is independent of the superficial two-phase velocity. Their results show that the product of the recirculation rate inner liquid slug and the slug residence time is a constant, which means that the product of the mass transfer rate and the residence time is also a constant. With the gas bubbles further moving downstream, the residence time becomes the dominant factor as the mass transfer rate largely decreases due to the smaller driving force (C^*-C), so the difference in $L_{B0}-L_B(x)$ becomes larger. Then at the final stage, $L_{B0}-L_B(x)$ decreases with the increase either in Q_G or Q_L, in spite of higher volumetric mass transfer coefficient under these conditions. It should be noted that with higher Q_G or Q_L, higher absorption flux is still obtained because the gas bubbles are more frequently generated and the velocities of them are much larger under these cases.

5. Conclusions

This paper focuses on a process analysis of CO_2 absorption in a microchannel with a T-junction. Visualization experiments using a high speed camera were performed to study the evolution of gas bubble sizes along the channel. First of all, the relationship between the total pressure drop of gas–liquid slug flow and the increase in bubble length was investigated. It was found that the pressure drop does not lead to a corresponding increase in bubble length based on the ideal gas law, which indicates that the pressure drop in single gas bubble is much lower than the two-phase pressure drop. This result validates the usage of bubble size reduction directly for determination of the mass transfer. A method based on the unit cell model was successfully developed to illustrate the bubble length evolution along the channel and determine the mass transfer coefficient. It takes advantage of its

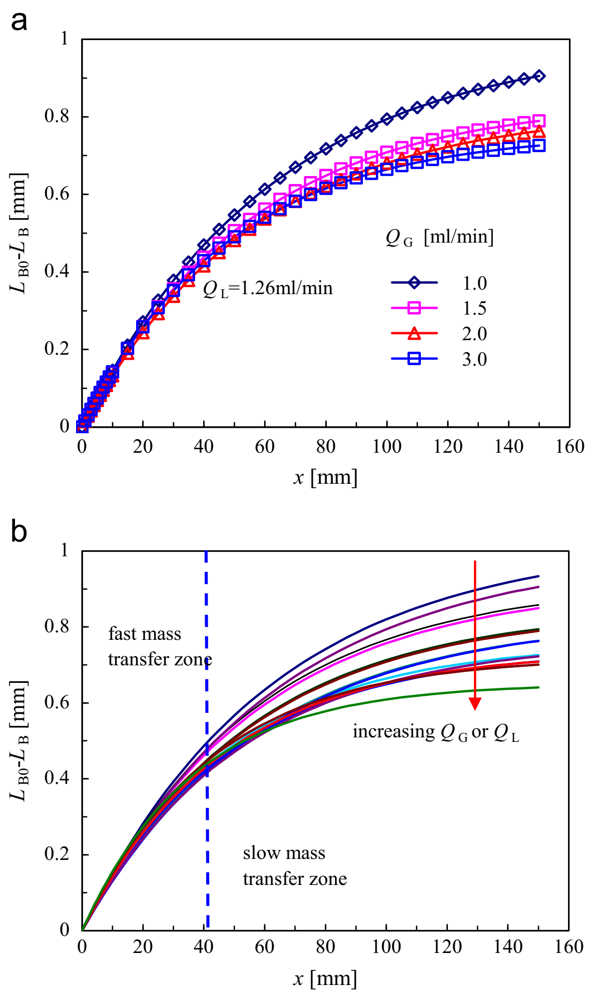

Fig. 16. Evolution of $L_{B0}-L_B(x)$ along the channel length for CO_2–H_2O system: (a) varying inlet gas flow rate at constant liquid flow rate and (b) varying experimental conditions.

convenience by eliminating extra efforts to exclude the end effect (Yue et al., 2007), which is useful in many practical applications.

Mass transfer coefficients under different fluid systems were measured. It has been found that the fluid properties have a significant effect on the mass transfer through influencing the flow hydrodynamics. However, the direct influence of fluid properties cannot be observed. Increasing the ethanol concentration leads to larger mass transfer coefficients because shorter gas bubbles and liquid slugs and larger bubble velocities are obtained. An empirical correlation was developed to predict the mass transfer coefficients with different fluid properties, which showed good performance. The amount of gas absorbed during the bubble formation process has been estimated to be about 2–10% of the inlet gas phase. The fraction φ linearly scales with the maximum mass transfer rate, which can be used to estimate the amount of gas absorbed during formation process. Despite the different initial bubble lengths, the reduction rate of the bubble size seems to be with very little difference for each fluid system at short distances (less than 40 mm) from the T-junction. The deviation of reduction rate becomes larger for longer distances when the effect of residence time is dominant over the mass transfer rate. The evolution of bubble size along the channel also gives us information of the gas removal efficiency, concentration in the liquid phase and the absorption flux. These features are very important for the reactor design and selection of optimal operation conditions.

Nomenclature

a	specific surface area, m^2/m^3
A	cross-sectional area, m^2
C	CO_2 concentration in water, mol/L
C^*	physical solubility of CO_2 in water, mol/L
Ca_{TP}	two phase capillary number defined by $(=\mu_L j_{TP}/\sigma_L)$, dimensionless
D_H	Hydrodynamic diameter, μm
f	bubble frequency, Hz
j	superficial velocity, m/s
k_L	liquid side mass transfer coefficient, m/s
k_La	liquid side volumetric mass transfer coefficient, s^{-1}
L	length
P	pressure, kPa
P_a	atmospheric pressure, kPa
Q	flow rates, mL/min
Q_a	mass flux over a reactor length, mL/min
R	gas constant, 8.3145 J/(K mol)
Re_G	superficial gas Reynolds number defined by $(=D_H j_G \rho_G/\mu_G)$
Re_L	superficial liquid Reynolds number defined by $(=D_H j_L \rho_L/\mu_L)$
Sc_L	liquid Schmidt number defined by $(=\mu_L/\rho_L D)$
Sh_L	liquid Sherwood number defined by $(=k_L D_H/D)$
T	temperature, K
U	velocity, m/s
W	channel width
We	two phase Weber number defined by $(=\rho_L {U_B}^2 D_H/\sigma_L)$, dimensionless
x	distance from the T-junction, mm

Subscripts

B	bubble
$B1$	the initial bubble
G	gas
L	liquid
S	slug

Acknowledgments

We acknowledge gratefully the financial supports for this project from the National Natural Science Foundation of China (Nos. 21225627, 21376234, and 91334201).

References

Abadie, T., Aubin, J., Legendre, D., Xuereb, C., 2012. Hydrodynamics of gas–liquid Taylor flow in rectangular microchannels. Microfluid. Nanofluid. 12, 355–369.
Abolhasani, M., Singh, M., Kumacheva, E., Günther, A., 2012. Automated microfluidic platform for studies of carbon dioxide dissolution and solubility in physical solvents. Lab Chip 12, 1611–1618.
Al-Rawashdeh, M., Nijhuis, X., Rebrov, E.V., Hessvel, V., Schouten, J.C., 2012. Design methodology for barrier-based two phase flow distributor. AIChE J. 58, 3482–3493.
Al-Rawashdeh, M., Zalucky, J., Muller, C., Nijhuis, T.A., Hessel, V., Schouten, J.C., 2013. Phenylacetylene hydrogenation over $[Rh(NBD)(PPh_3)_2]BF_4$ catalyst in a numbered-up microchannels reactor. Ind. Eng. Chem. Res. 52, 11516–11526.
Berčič, G., Pintar, A., 1997. The role of gas bubbles and liquid slug lengths on mass transport in the Taylor flow through capillaries. Chem. Eng. Sci. 52, 3709–3719.
Cao, H., Chen, G., Yuan, Q., 2010. Thermal performance of crossflow microchannel heat exchangers. Ind. Eng. Chem. Res. 49, 6215–6220.
Cubaud, T., Sauzade, M., Sun, R., 2012. CO_2 dissolution in water using long serpentine microchannels. Biomicrofluidics 6, 022002.
Dalmolin, I., Skovroinski, E., Biasi, A., Corazza, M.L., Dariva, C., Oliveira, J.V., 2006. Solubility of carbon dioxide in binary and ternary mixtures with ethanol and water. Fluid Phase Equilib. 245, 193–200.
Dang, M., Yue, J., Chen, G., Yuan, Q., 2013. Formation characteristics of Taylor bubbles in a microchannel with a converging shape mixing junction. Chem. Eng. J. 223, 99–109.

Dietrich, N., Loubière, K., Jimenez, M., Hébrard, G., Gourdon, C., 2013. A new direct technique for visualizing and measuring gas–liquid mass transfer around bubbles moving in a straight millimetric square channel. Chem. Eng. Sci. 100, 172–182.

Fries, D., Waelchli, S., Rudolfvonrohr, P., 2008a. Gas–liquid two-phase flow in meandering microchannels. Chem. Eng. J. 135, S37–S45.

Fries, D.M., Trachsel, F., von Rohr, P.R., 2008b. Segmented gas–liquid flow characterization in rectangular microchannels. Int. J. Multiph. Flow 34, 1108–1118.

Günther, A., Khan, S.A., Thalmann, M., Trachsel, F., Jensen, K.F., 2004. Transport and reaction in microscale segmented gas–liquid flow. Lab Chip 4, 278–286.

Ganapathy, H., Al-Hajri, E., Ohadi, M., 2013. Mass transfer characteristics of gas–liquid absorption during Taylor flow in mini/microchannel reactors. Chem. Eng. Sci. 101, 69–80.

Garstecki, P., Fuerstman, M.J., Stone, H.A., Whitesides, G.M., 2006. Formation of droplets and bubbles in a microfluidic T-junction-scaling and mechanism of break-up. Lab Chip 6, 437–446.

Han, Y., Shikazono, N., 2009. Measurement of liquid film thickness in micro square channel. Int. J. Multiph. Flow 35, 896–903.

Hessel, V., Kralisch, D., Kockmann, N., Noël, T., Wang, Q., 2013. Novel process windows for enabling, accelerating, and uplifting flow chemistry. ChemSusChem 6, 746–789.

Kawahara, A., Sadatomi, M., Okayama, K., Kawaji, M., Chung, P.M.Y., 2005. Effects of channel diameter and liquid properties on void fraction in adiabatic two-phase flow through microchannels. Heat Transf. Eng. 26, 13–19.

Khattab, I.S., Bandarkar, F., Fakhree, M.A.A., Jouyban, A., 2012. Density, viscosity, and surface tension of water + ethanol mixtures from 293 to 323 K. Korean J. Chem. Eng. 29 (6), 812–817.

Kreutzer, M.T., Kapteijn, F., Moulijn, J.A., Heiszwolf, J.J., 2005a. Multiphase monolith reactors: chemical reaction engineering of segmented flow in microchannels. Chem. Eng. Sci. 60, 5895–5916.

Kreutzer, M.T., Kapteijn, F., Moulijn, J.A., Kleijn, C.R., Heiszwolf, J.J., 2005b. Inertial and interfacial effects on pressure drop of Taylor flow in capillaries. AIChE J. 51, 2428–2440.

Kuhn, S., Jensen, K.F., 2012. A pH-sensitive laser-induced fluorescence technique to monitor mass transfer in multiphase flows in micro fluidic devices. Ind. Eng. Chem. Res. 51, 8999–9006.

Li, W., Liu, K., Simms, R., Greener, J., Jagadeesan, D., Pinto, S., Gunther, A., Kumacheva, E., 2012. Microfluidic study of fast gas–liquid reactions. J. Am. Chem. Soc. 134, 3127–3132.

Pohorecki, R., 2007. Effectiveness of interfacial area for mass transfer in two-phase flow in microreactors. Chem. Eng. Sci. 62, 6495–6498.

Qian, D., Lawal, A., 2006. Numerical study on gas and liquid slugs for Taylor flow in a T-junction microchannel. Chem. Eng. Sci. 61, 7609–7625.

Simons, J., Ponter, A.B., 1975. Diffusivity of carbon dioxide in ethanol–water mixtures. J. Chem. Eng. Jpn. 8 (5), 347–350.

Sobieszuk, P., Aubin, J., Pohorecki, R., 2012. Hydrodynamics and mass transfer in gas–liquid flows in microreactors. Chem. Eng. Technol. 35, 1346–1358.

Sobieszuk, P., Pohorecki, R., Cygański, P., Grzelka, J., 2011. Determination of the interfacial area and mass transfer coefficients in the Taylor gas–liquid flow in a microchannel. Chem. Eng. Sci. 66, 6048–6056.

Sun, R., Cubaud, T., 2011. Dissolution of carbon dioxide bubbles and microfluidic multiphase flows. Lab Chip 11, 2924–2928.

Tan, J., Lu, Y.C., Xu, J.H., Luo, G.S., 2012a. Mass transfer characteristic in the formation stage of gas–liquid segmented flow in microchannel. Chem. Eng. J. 185–186, 314–320.

Tan, J., Lu, Y.C., Xu, J.H., Luo, G.S., 2012b. Mass transfer performance of gas–liquid segmented flow in microchannels. Chem. Eng. J. 181–182, 229–235.

Thulasidas, T.C., Abraham, M.A., Cerro, R.L., 1995. Bubble-train flow in capillaries of circular and square cross-section. Chem. Eng. Sci. 50, 183–199.

Triplett, K.A., Ghiaasiaan, S.M., Abdel-Khalik, S.I., Sadowski, D.L., 1999. Gas–liquid two-phase flow in microchannels – Part I: two-phase flow patterns. Int. J. Multiph. Flow 25, 377–394.

van Baten, J.M., Krishna, R., 2004. CFD simulations of mass transfer from Taylor bubbles rising in circular capillaries. Chem. Eng. Sci. 59, 2535–2545.

van Steijn, V., Kreutzer, M.T., Kleijn, C.R., 2007. μ-PIV study of the formation of segmented flow in microfluidic T-junctions. Chem. Eng. Sci. 62, 7505–7514.

Vandu, C.O., Liu, H., Krishna, R., 2005. Mass transfer from Taylor bubbles rising in single capillaries. Chem. Eng. Sci. 60, 6430–6437.

Xiong, R., Chung, J.N., 2007. An experimental study of the size effect on adiabatic gas–liquid two-phase flow patterns and void fraction in microchannels. Phys. Fluids 19, 033301.

Yao, C., Zhao, Y., Ye, C., Minhui, D., Dong, Z., Chen, G., 2013. Characteristics of slug flow with inertial effects in a rectangular microchannel. Chem. Eng. Sci. 95, 246–256.

Yue, J., Chen, G., Yuan, Q., Luo, L., Gonthier, Y., 2007. Hydrodynamics and mass transfer characteristics in gas–liquid flow through a rectangular microchannel. Chem. Eng. Sci. 62, 2096–2108.

Yue, J., Luo, L., Gonthier, Y., Chen, G., Yuan, Q., 2008. An experimental investigation of gas–liquid two-phase flow in single microchannel contactors. Chem. Eng. Sci. 63, 4189–4202.

Yue, J., Luo, L., Gonthier, Y., Chen, G., Yuan, Q., 2009. An experimental study of air–water Taylor flow and mass transfer inside square microchannels. Chem. Eng. Sci. 64, 3697–3708.

Zaloha, P., Kristal, J., Jiricny, V., Völkel, N., Xuereb, C., Aubin, J., 2012. Characteristics of liquid slugs in gas–liquid Taylor flow in microchannels. Chem. Eng. Sci. 68, 640–649.

Zhao, Y., Chen, G., Ye, C., Yuan, Q., 2013. Gas–liquid two-phase flow in microchannel at elevated pressure. Chem. Eng. Sci. 87, 122–132.